Preclinical Evaluation of ^{86}Y-Labeled Inhibitors of Prostate-Specific Membrane Antigen for Dosimetry Estimates

Sangeeta Ray Banerjee[1], Catherine A. Foss[1], Mrudula Pullambhatla[1], Yuchuan Wang[1], Senthamizhchelvan Srinivasan[1], Robert F. Hobbs[1], Kwamena E. Baidoo[2], Martin W. Brechbiel[2], Sridhar Nimmagadda[1], Ronnie C. Mease[1], George Sgouros[1], and Martin G. Pomper[1]

[1]*The Russell H. Morgan Department of Radiology and Radiological Science, Johns Hopkins University, Baltimore, Maryland; and* [2]*National Institutes of Health, Bethesda, Maryland*

^{86}Y (half-life = 14.74 h, 33% β^+) is within an emerging class of positron-emitting isotopes with relatively long physical half-lives that enables extended imaging of biologic processes. We report the synthesis and evaluation of 3 low-molecular-weight compounds labeled with ^{86}Y for imaging the prostate-specific membrane antigen (PSMA) using PET. Impetus for the study derives from the need to perform dosimetry estimates for the corresponding ^{90}Y-labeled radiotherapeutics. **Methods:** Multistep syntheses were used in preparing ^{86}Y-**4**–**6.** PSMA inhibition constants were evaluated by competitive binding assay. In vivo characterization using tumor-bearing male mice was performed by PET/CT for ^{86}Y-**4**–**6** and by biodistribution studies of ^{86}Y-**4** and ^{86}Y-**6** out to 24 h after injection. Quantitative whole-body PET scans were recorded to measure the kinetics for 14 organs in a male baboon using ^{86}Y-**6. Results:** Compounds ^{86}Y-**4**–**6** were obtained in high radiochemical yield and purity, with specific radioactivities of more than 83.92 GBq/μmol. PET imaging and biodistribution studies using PSMA-positive PC-3 PIP and PSMA-negative PC-3 flu tumor-bearing mice revealed that ^{86}Y-**4**–**6** had high site-specific uptake in PSMA-positive PC-3 PIP tumor starting at 20 min after injection and remained high at 24 h. Compound ^{86}Y-**6** demonstrated the highest tumor uptake and retention, with 32.17 ± 7.99 and 15.79 ± 6.44 percentage injected dose per gram (%ID/g) at 5 and 24 h, respectively. Low activity concentrations were associated with blood and normal organs, except for the kidneys, a PSMA-expressing tissue. PET imaging in baboons reveals that all organs have a 2-phase (rapid and slow) clearance, with the highest uptake (8 %ID/g) in the kidneys at 25 min. The individual absolute uptake kinetics were used to calculate radiation doses using the OLINDA/EXM software. The highest mean absorbed dose was received by the renal cortex, with 1.9 mGy per MBq of ^{86}Y-**6. Conclusion:** Compound ^{86}Y-**6** is a promising candidate for quantitative PET imaging of PSMA-expressing tumors. Dosimetry calculations indicate promise for future ^{90}Y or other radiometals that could use a similar chelator/scaffold combination for radiopharmaceutical therapy based on the structure of **6.**

Received Sep. 25, 2014; revision accepted Jan. 21, 2015.
For correspondence or reprints contact either of the following:
Martin G. Pomper, Johns Hopkins Medical School, 600 N. Wolfe St., Baltimore, MD 21287.
E-mail: mpomper@jhmi.edu
Sangeeta Ray Banerjee, Johns Hopkins Medical School, 1550 Orleans St., CRBII, Rm. 470, Baltimore, MD 21231.
E-mail: sray9@jhmi.edu
Published online Feb. 26, 2015.

Key Words: PSMA; PET; ^{86}Y-DOTA; molecular imaging; radiopharmaceutical therapy

J Nucl Med 2015; 56:628–634
DOI: 10.2967/jnumed.114.149062

The positron-emitting radionuclide ^{86}Y (half-life [$t_{1/2}$] = 14.74 h, β^+ = 33%, energy of the positron [$E_{\beta+}$] = 664 keV) is an attractive isotope for molecular imaging (*1*). ^{86}Y can readily be prepared on a small biomedical cyclotron using the ^{86}Sr(p, n)^{86}Y nuclear reaction (*2*). The extensive use of the high-energy β^--emitter ^{90}Y ($t_{1/2}$ = 64.06 h, β^- = 72%, β particle energy [$E_{\beta}{}^-$] = 2.288 MeV) for endoradiotherapy (*3,4*) makes ^{86}Y ideal for dosimetry estimates of ^{90}Y-labeled radiotherapeutics (*5*). Antibodies and peptides radiolabeled with ^{86}Y have properties identical to those labeled with ^{90}Y, enabling accurate absorbed dose estimates for ^{90}Y for radiotherapeutics (*1,6*).

The prostate-specific membrane antigen (PSMA) is increasingly recognized as a viable target for imaging and therapy of prostate and other forms of cancer (*7–9*). We and others have demonstrated PSMA-targeted radionuclide imaging in experimental models of prostate cancer (*10–12*) and in the clinic (*13–15*) using functionalized cysteine-glutamate or lysine-glutamate ureas. For the attachment of large molecular fragments, such as radiometal (^{99m}Tc, ^{68}Ga, ^{111}In) complexes (*16–18*) and nanoparticles (*19,20*), a long linker was placed between the large molecule and the targeting urea to retain PSMA-targeted binding. On the basis of those initial positive results, we and others have reasoned that urea-based agents could also be used for radiotherapy of PSMA-containing lesions using radionuclides. In fact, clinical studies using that approach with ^{131}I-MIP1095 ((*S*)-2-(3-((*S*)-1-carboxy-5-(3-(4-^{131}I-iodophenyl)ureido) pentyl)ureido)pentanedioicacid) (*15*) and ^{177}Lu-labeled PSMA-targeted agents (*14*) are under way for the treatment of castrate-resistant prostate cancer. Although ^{177}Lu has a shorter β-particle range ($t_{1/2}$ = 6.7 d, $E_{\beta}{}^-$ = 0.5 MeV) than ^{90}Y, because they have similar chelation chemistry, we proposed ^{86}Y as a suitable imaging surrogate to investigate potential ^{177}Lu-based radiotherapeutics as well as those radiolabeled with ^{90}Y. A similar rationale has been applied to agents for neuroendocrine-targeted peptide receptor radionuclide therapy (*21*). The aim of this study was to prepare and investigate the biodistribution of three ^{86}Y-labeled PSMA-binding ureas (Fig. 1) in a rodent experimental model and image the most pharmacokinetically favorable agent in nonhuman primates

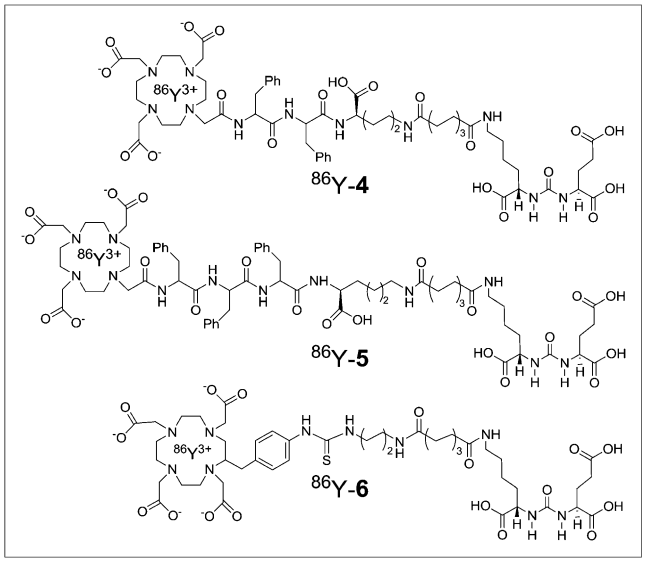

FIGURE 1. ^{86}Y-labeled inhibitors of PSMA.

for radiation dosimetry in preparation for clinical trials with the corresponding ^{90}Y- and ^{177}Lu-labeled agents.

MATERIALS AND METHODS

Detailed chemical and radiochemical syntheses of $^{86/89}$Y-**4,** $^{86/89}$Y-**5,** and $^{86/89}$Y-**6** (Fig. 1) are provided in the supplemental materials (available online at http://jnm.snmjournals.org). PSMA inhibitory activities were determined using a fluorescence-based assay (*17*). Enzyme inhibitory constants (K_i values) were generated using the Cheng–Prusoff conversion (*22*). Sublines of the androgen-independent PC-3 human prostate cancer xenograft were used (*17*). Those sublines have been modified to express high (PC-3 PIP) or naturally produce low (PC-3 flu) levels of PSMA and were generously provided by Dr. Warren Heston (Cleveland Clinic). Details related to cell culture and animal models are included in the supplemental materials. Six- to 8-wk-old male, nonobese diabetic/severe-combined immunodeficient mice (Charles River Laboratories) were implanted subcutaneously with PSMA-positive (PSMA+) PC-3 PIP and PSMA-negative (PSMA−) PC-3 flu cells (2×10^6 in 100 μL of Matrigel [BD Biosciences]) at the cephalad right and left flanks, respectively. Mice were imaged or used in biodistribution assays when the xenografts reached 5–7 mm in diameter. Details of the biodistribution assay are included in the supplemental materials.

TABLE 1
PSMA Inhibitory Activities

Compound	K_i (nM)	95% confidence interval of K_i
4	0.41	0.34–0.56
^{89}Y-**4**	0.36	0.2–0.51
5	3.12	1.7–5.60
^{89}Y-**5**	0.10	0.04–0.32
6	1.80	0.83–3.92
^{89}Y-**6**	2.99	1.91–4.69
ZJ43	1.16	0.08–2.26

Animal Imaging

Small-Animal PET and CT. Dynamic, whole-body PET and CT images were acquired on an eXplore VISTA small-animal PET system (GE Healthcare) and an X-SPECT small-animal SPECT/CT system (Gamma Medica Ideas), respectively, with details presented in the supplemental materials.

*Papio Anubis (Baboon) PET Imaging of ^{86}Y-**6**.* A male *Papio anubis* (8 y, 27.1 kg) was used to study the biodistribution of ^{86}Y-**6.** Nine static PET images were acquired at 5, 10, 15, 20, and 35 min as well as at 1, 2, 3.5, and 23 h after intravenous administration of 80.7 MBq (2.2 mCi) of ^{86}Y-**6** as a bolus. Images were acquired in 2-dimensional mode on a Discovery RX VCT scanner (GE Healthcare). Details related to imaging and analyses are provided in the supplemental materials.

Radiation Dosimetry

Related equations, explanation, and assumptions for dosimetry calculation can be found in the supplemental materials. Measured activity concentration (in Bq/cm^3) values per time point per organ were decay-corrected and divided by the baboon organ mass, determined by the CT density and volume from the drawn contours, and the injected radioactivity to obtain the fraction of initial radioactivity per gram (FIA/g) for each time point and each organ. The baboon FIA/g values were then converted to human FIA (per organ) using the related equation (*23,24*). The resulting human FIA values were then plotted as a function of time and fit to a biexponential expression, and the value for the time-integrated activity coefficient (previously known as residence time (*25*)) for each source organ was calculated. Radiation absorbed doses were obtained by converting time-integrated activity to absorbed doses according to the MIRD absorbed-fraction methodology (*25*) through the use of the OLINDA/EXM software (*26*).

RESULTS

The chemical structures of the ^{86}Y-labeled PSMA-targeting compounds ^{86}Y-**4,** ^{86}Y-**5,** and ^{86}Y-**6** are shown in Figure 1. Radiolabeling of the target compounds proceeded in high yield (~90%–97%) and radiochemical purity (>98%), with a high specific radioactivity (>83.92 GBq/μmol [2.27 Ci/μmol]). All compounds displayed high binding affinity, with K_i values ranging from 0.10 to 4.69 nM (Table 1).

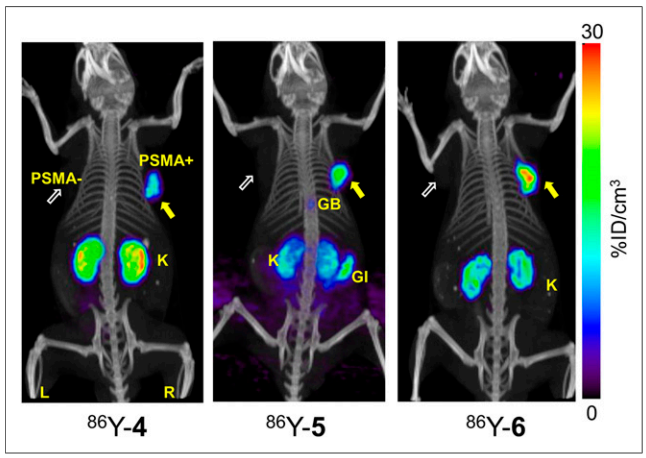

FIGURE 2. Whole-body PET/CT images of ^{86}Y-**4,** ^{86}Y-**5,** and ^{86}Y-**6** in mice bearing PSMA+ PC3 PIP and PSMA− PC3 flu tumors at 2 h after injection. Mice were injected with approximately 3.3 MBq (90 μCi) of radiotracer intravenously. Images are decay-corrected and scaled to the same maximum value. GB = gallbladder; GI = gastrointestinal tract; K = kidney.

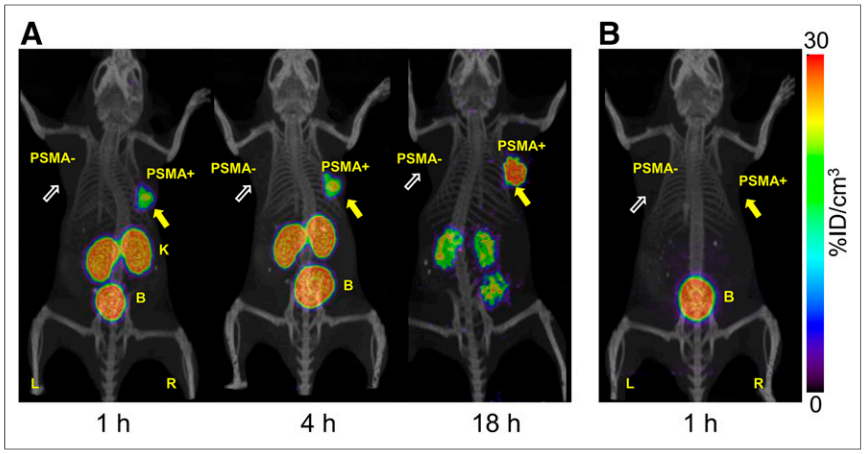

FIGURE 3. PET/CT images of ^{86}Y-**4** in mice bearing PSMA+ PC3 PIP and PSMA− PC3 flu tumors. Images obtained without (A) and with (B) blockade of PSMA using the potent, selective PSMA inhibitor **ZJ43** as blocking agent (50 mg/kg). Reduction of radiotracer uptake in both tumor and kidneys (another PSMA+ site) on cotreatment with **ZJ43** provided a further check on PSMA-specific binding. Mice were injected with approximately 6.2 MBq (168 μCi) of radiotracer intravenously. Images are decay-corrected and scaled to the same maximum value. B = bladder; K = kidney.

Small-Animal PET Imaging

Whole-body PET/CT images were obtained for ^{86}Y-**4,** ^{86}Y-**5,** and ^{86}Y-**6** (Figs. 2–4). All 3 radiotracers enabled visualization of PSMA+ PC-3 PIP tumor and kidneys (Fig. 2), a known PSMA-expressing organ, at 2 h after injection. Renal uptake of the radiotracers is partially due to the route of excretion of these agents and to specific uptake from the expression of PSMA in mouse proximal renal tubules (*27*). Agent ^{86}Y-**5** demonstrated nonspecific accumulation in the gastrointestinal tract, presumably due to the increased hydrophobicity from the 3 phenylalanine residues on the linker moiety. PET/CT images of ^{86}Y-**4** were acquired at 1, 4, and 18 h after injection considering the short biologic half-life of this class of low-molecular-weight compounds. The presence of the radiotracer in PSMA+ PC-3 PIP tumor, kidneys, and urinary bladder was observed up to 4 h (Fig. 3A). Radioactivity in the bladder and kidneys cleared significantly by 18 h, although the PSMA+ PC-3 PIP tumor retained some activity. As a further test of in vivo binding specificity, we performed a blocking study of ^{86}Y-**4** by pretreating the animal with the potent, selective PSMA inhibitor **ZJ43** (50 mg/kg) (*28*). Figure 3B demonstrates that **ZJ43** was capable of blocking the binding of ^{86}Y-**4** not only within tumor but also within the renal cortex, another PSMA-expressing tissue (*27*). Figure 4 displays PET/CT images of ^{86}Y-**6** to 12 h after injection. Significantly, ^{86}Y-**6** exhibited faster clearance of radioactivity from normal tissues, and by 12 h after injection radioactivity was largely cleared from the kidneys, producing clear tumor-to-background contrast. Clear delineation of PSMA+ PC-3 PIP tumor was achieved as early as at 15 min after injection. Notably, ^{86}Y-**6** does not contain the additional phenylalanine moieties of ^{86}Y-**4** and ^{86}Y-**5** and uses a *p*-isothiocyanatobenzyl DOTA chelator, which adds an additional carboxylate to hold the metal strongly and decreases lipophilicity.

Biodistribution in Mice

On the basis of the results of imaging, compounds ^{86}Y-**4** and ^{86}Y-**6** were further assessed in a standard biodistribution assay (*17*). Tables 2 and 3 show the percentage injected dose per gram (%ID/g) uptake values in selected organs at 1, 2, 5, and 24 h after injection. Both radiotracers showed PSMA-dependent binding in PSMA+ PC-3 PIP tumor xenografts, with ^{86}Y-**4** demonstrating high tumor uptake at as early as 1 h after injection (29.3 ± 8.7 %ID/g) with relatively slow clearance to 15.7 ± 1.7 %ID/g at 5 h and to 5.9 ± 0.8 %ID/g at 24 h after injection. PSMA+ PC-3 PIP tumor to PSMA− PC-3 flu tumor uptake ratios ranged from 89 at 1 h to a high of 229 at 24 h. Blood and normal tissues such as the heart, liver, stomach, and pancreas did not show significant uptake (~1 %ID/g) and decreased below 0.02 %ID/g after 24 h. PSMA+ PC-3 PIP tumor-to-muscle ratios were also high, achieving a maximum value of 1,046 at 24 h. Kidney uptake was found expectedly high and peaked at 244.9 ± 8.8 %ID/g at 1 h and decreased to 1.5 ± 0.7 %ID/g by 24 h.

Table 3 shows the organ %ID/g uptake values for ^{86}Y-**6.** Compound ^{86}Y-**6** quickly accumulated within the PSMA+ PC-3 PIP tumor within 1 h after injection, with an uptake value of 26.6 ± 1.9 %ID/g. The radiotracer concentration continuously increased within PSMA+ PC-3 PIP tumor to exhibit the highest uptake of 32.2 ± 8.0 %ID/g at 5 h after injection. Tumor uptake remained high until 24 h after injection. Normal organs such as the blood, heart, liver, spleen, stomach, and pancreas exhibited low uptake at 1 h, which decreased to below 0.4 %ID/g by 5 h. Renal uptake for ^{86}Y-**6,** 86.5 ± 13.6 and 54.0 ± 9.2 %ID/g at 1 and 2 h, respectively, was much lower than for ^{86}Y-**4.**

Baboon PET Imaging and Pharmacokinetics of ^{86}Y-6

Figure 5 depicts the baboon PET study, for which radiotracer is seen in the liver, salivary glands, kidney, and bladder. For whole kidney, renal cortex, and prostate, contours were drawn on each PET image for quantification. All organs showed 2-phase (rapid and slow) biologic clearance. The kidneys had the highest uptake at about 25 min after injection (8 %ID/g). Sixty-eight percent of

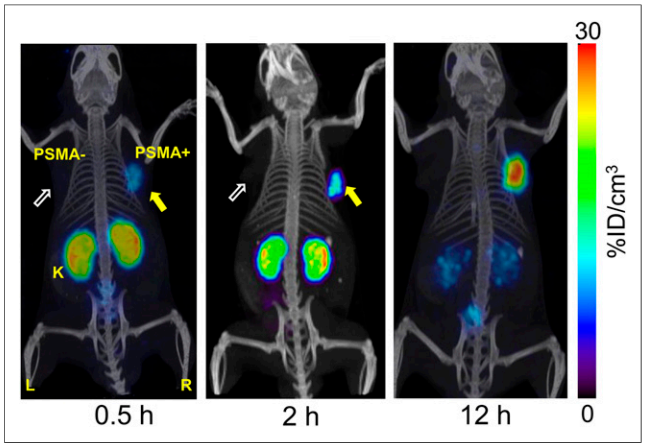

FIGURE 4. PET/CT images of ^{86}Y-**6** in mice bearing PSMA+ PC3 PIP and PSMA− PC3 flu tumors. Mice were injected with approximately 6.2 MBq (160 μCi) of radiotracer intravenously. Images are decay-corrected and scaled to same maximum value. K = kidney.

TABLE 2
Biodistribution of ^{86}Y-**4** in Mice (%ID/g)

Tissue	1 h	2 h	5 h	24 h
Blood	0.5 ± 0.2	0.1 ± 0.1	0.0 ± 0.0	0.0 ± 0.0
Heart	0.3 ± 0.1	0.1 ± 0.0	0.0 ± 0.0	0.0 ± 0.0
Lung	1.1 ± 0.2	0.3 ± 0.1	0.1 ± 0.0	0.0 ± 0.0
Liver	0.2 ± 0.1	0.1 ± 0.0	0.1 ± 0.0	0.0 ± 0.0
Spleen	5.1 ± 1.4	1.3 ± 0.5	0.2 ± 0.1	0.0 ± 0.0
Kidney	245.0 ± 9.0	123.0 ± 48	23.0 ± 9.7	1.5 ± 0.7
Muscle	0.5 ± 0.4	0.1 ± 0.1	0.1 ± 0.1	0.0 ± 0.0
Small intestines	0.2 ± 0.0	0.1 ± 0.0	0.0 ± 0.0	0.0 ± 0.0
Large intestines	0.3 ± 0.1	0.1 ± 0.0	0.1 ± 0.0	0.0 ± 0.0
Bladder	1.5 ± 0.8	12.6 ± 12.5	3.6 ± 1.	0.2 ± 0.2
PC-3 PIP	29.0 ± 8.7	21.6 ± 3.6	15.7 ± 1.7	5.9 ± 0.8
PC-3 flu	0.3 ± 0.1	0.1 ± 0.0	0.1 ± 0.0	0.0 ± 0.0
PIP to flu	89	164	156	229
PIP to blood	55	198	624	2,352
PIP to muscle	54	140	191	1,046

the radioactivity seen in the kidneys was cleared with a biologic half-life of about 1 h (0.84 h), and the remaining radioactivity was cleared with a biologic half-life of 16.6 h. Most (66%) of the radioactivity in the renal cortex was cleared with a biologic half-life of 1.1 h, and the remaining radioactivity was cleared with a biologic half-life of about 19 h. Significant uptake and retention were seen in the liver and salivary glands, although milder compared with PET scans of patients imaged with ^{68}Ga-labeled PSMA-targeted agents and $^{124/131}$I-MIP-1095 (*15*). Supplemental Table 1 gives the summary of the biologic clearance kinetics of all organs. The time-integrated activity coefficients used in the dose calculations are listed in Supplemental Table 2.

Organ-Absorbed Doses

Table 4 provides a detailed list of the organ-absorbed doses, expressed in units of mGy/MBq, for ^{86}Y and ^{90}Y/^{177}Lu. For all isotopes, the renal cortex received the highest absorbed dose per unit activity. Accordingly, it is likely that the renal cortex would be the

TABLE 3
Biodistribution of ^{86}Y-**6** in Mice (%ID/g)

Tissue	1 h	2 h	5 h	24 h
Blood	0.6 ± 0.0	0.2 ± 0.0	0.1 ± 0.0	0.0 ± 0.0
Heart	0.3 ± 0.0	0.1 ± 0.0	0.0 ± 0.0	0.0 ± 0.0
Lung	1.1 ± 0.2	0.5 ± 0.1	0.2 ± 0.0	0.1 ± 0.0
Liver	0.3 ± 0.0	0.2 ± 0.0	0.1 ± 0.0	0.1 ± 0.0
Stomach	0.3 ± 0.1	0.14 ± 0.01	0.11 ± 0.01	0.05 ± 0.09
Pancreas	0.3 ± 0.1	0.23 ± 0.2	0.08 ± 0.04	0.01 ± 0.01
Spleen	3.0 ± 0.7	1.31 ± 0.7	0.36 ± 0.12	0.11 ± 0.05
Fat	0.6 ± 0.5	1.87 ± 3.44	0.12 ± 0.17	0.01 ± 0.01
Kidney	87.0 ± 14.0	54.0 ± 9.0	15.6 ± 4.1	4.8 ± 0.8
Muscle	0.8 ± 1.2	0.25 ± 0.2	0.0 ± 0.0	0.0 ± 0.0
Small intestines	0.3 ± 0.1	0.1 ± 0.0	0.07 ± 0.02	0.02 ± 0.02
Large intestines	0.4 ± 0.3	0.2 ± 0.1	0.1 ± 0.	0.0 ± 0.0
Bladder	6.0 ± 3.9	5.5 ± 3.7	0.8 ± 0.1	0.4 ± 0.3
PC-3 PIP	26.6 ± 1.9	29.2 ± 2.3	32.2 ± 8.0	15.8 ± 6.4
PC-3 flu	0.4 ± 0.1	0.2 ± 0.0	0.2 ± 0.1	0.1 ± 0.1
PIP to flu	66	152	183	130
PIP to blood	44	145	378	620
PIP to muscle	33	115	921	3,010

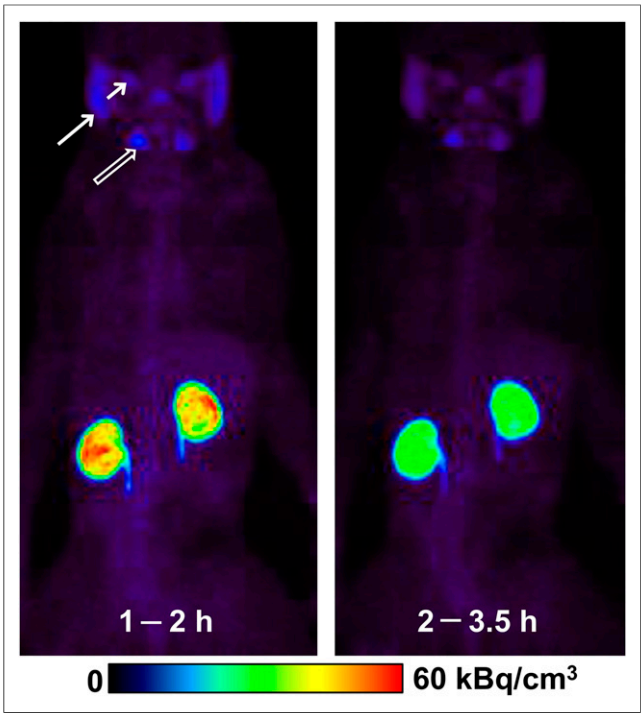

FIGURE 5. Three-dimensional time course maximum-intensity reprojection display of ^{86}Y-**6** PET in baboon. To enhance visualization, bladder radioactivities were segmented semiautomatically using a thresholding method and subsequently removed. Maximum-intensity reprojection 3-dimensional rendering was used to provide an overview of whole-body radiotracer distribution. Little radiotracer was observed in most normal tissues except for bladder (not shown) and kidney (K). Animal was catheterized for this study. Mild uptake in lacrimal glands, parotids, and salivary glands was noted (short, long, and unfilled arrows, respectively).

dose-limiting organ for therapeutic radiometals in the context of patient-specific absorbed dose treatment planning (*29,30*), followed by the bladder. For the diagnostic isotope ^{86}Y, an effective dose of 0.099 mSv/MBq was also calculated in OLINDA/EXM.

DISCUSSION

We have synthesized and evaluated three ^{86}Y-labeled, PSMA-targeted agents to undertake nonhuman primate dosimetry. Those compounds contain a DOTA or DOTA mono-amide chelated radiometal attached to the targeting urea similar to others we have published (*12,17*). We have focused on DOTA and its derivatives because they can be used both for PET (^{86}Y) and for radiopharmaceutical therapy (^{90}Y). It has been documented that pharmacokinetics are dependent on the radiometal chelator used, including those for compounds specifically designed to bind to PSMA. That is primarily attributed to the overall charge of the radioligand and the stability of the metal chelate complexes. Specifically, in our previous report of ^{68}Ga-labeled PSMA-binding DOTA-conjugated agents, ^{68}Ga-**4** demonstrated the fastest clearance from normal tissues, including the kidneys (*12*). However, in the current study we observed that ^{86}Y-**4** exhibited unexpectedly higher renal uptake and may not be a suitable candidate for radiotherapy. The evaluation of ^{86}Y-**6** demonstrated the desired lower kidney uptake and higher tumor retention required for radiotherapy and was subsequently selected for quantitative PET imaging in a baboon for dosimetry measurements.

The binding specificity study (Fig. 3B) indicated that at 1 h nearly all renal binding of ^{86}Y-**4** was specific rather than due to excretion. Evidence suggests that more organized and rapid blood flow in renal parenchyma, compared with tumors, may account for longer tumor rather than renal retention for many of these agents. Although PSMA-binding affinity is 1 factor that likely determines tumor versus renal uptake, other factors, such as lipophilicity, charge, plasma protein binding, and molecular weight, likely also play significant roles. The estimated renal cortex doses of 1.19 mGy/MBq for ^{90}Y and 0.245 mGy/MBq for ^{177}Lu compare favorably with the values of 1.97 mGy/MBq for ^{90}Y and 0.45 mGy/MBq for ^{177}Lu calculated in a report involving peptide receptor radiation therapy (*29*), for which the renal cortex was the dose-limiting organ. However, several caveats to the absorbed dose calculations must be made. First, the organ uptake measurements from PET are predominantly at early time points (median, 35 min; final time point, 3.5 h), and the time points through numerous organs are mostly short (median, 35 min; eighth time point, 3.5 h), raising questions regarding the accuracy of translating the results to the longer-lived isotopes such as ^{90}Y ($t_{1/2}$ = 64 h) and particularly ^{177}Lu ($t_{1/2}$ = 6.72 d). It is a problem faced by all theranostics that the surrogate has a significantly shorter half-life than the therapeutic. Second, the chelation stability of nonidentical therapeutic radionuclides, ^{177}Lu, for example, relative to that of ^{86}Y and the fate of the therapeutic radionuclide if the agent is internalized must also be taken into consideration. Cellular retention and residualization of chelated ^{90}Y after internalization has also been well demonstrated (*31*).

The commonly used and clinically implemented chelating agent DOTA was used for all 3 radioligands because DOTA, and many DOTA derivatives, is known to form kinetically and thermodynamically stable complexes. The corresponding Y(III) complex has been shown in many cases to be stable in vivo, a desirable trait for a chelator. Significantly, DOTA is also reported to form stable complexes with an array of trivalent metal ions including lanthanides, for example, ^{177}Lu(III), and actinides, for example, ^{225}Ac(III), which are chemically disparate to ^{86}Y(III). Moreover, PSMA-binding urea-based agents are stable under the radiolabeling conditions used for DOTA, so we have not pursued other chelators such as cyclohexyl-diethylenetriaminepentaacetic acid (CHX-A″-DTPA) (*32*) presently.

Recently, ^{90}Y- or ^{177}Lu-labeled versions of the PSMA-targeted monoclonal antibody J591 demonstrated promising results in phase I and II clinical trials (*33–35*). In those cases, ^{111}In-labeled antibody was used for dosimetry calculations (*36*). Although those radiolabeled monoclonal antibodies hold potential for tumor detection and therapy, their modest tumor targeting and a relatively high absorbed dose to red marrow militate against routine clinical use. As an alternative approach, early clinical results using ^{131}I-labeled PSMA-targeted, urea-based small molecules exhibited high dose delivery to malignant foci (*15*). In those published studies, the salivary glands showed the highest absorbed doses (4.62 mGy/MBq), followed by both liver (1.47 mGy/MBq) and kidneys (1.45 mGy/MBq) (*15*). It is probable that a significant contributor to the salivary gland absorbed dose is free iodine uptake, as also evidenced by the relatively high (0.91 mGy/MBq) thyroid absorbed dose, which does not occur in the current study. In general, the clearance rates from normal organs are more rapid for ^{86}Y-**6** than for the published results (*15*), with the exception of the kidneys.

TABLE 4
Organ-Absorbed Doses in Reference Adult Male Based on Baboon PET Imaging Data

Target organ	Organ doses (mGy/MBq)		
	^{86}Y	^{177}Lu	^{90}Y
Adrenals	8.62E−02	6.96E−03	3.46E−02
Brain	2.30E−02	1.48E−03	6.79E−03
Breasts	4.52E−02	6.08E−03	3.46E−02
Gallbladder wall	7.88E−02	6.79E−03	3.46E−02
Lower large intestine wall	9.61E−02	7.06E−03	3.46E−02
Small intestine	8.72E−02	8.30E−03	4.29E−02
Stomach wall	6.69E−02	7.88E−03	3.46E−02
Upper large intestine wall	8.56E−02	1.16E−02	6.29E−02
Heart wall	6.70E−02	9.54E−03	5.33E−02
Kidneys	4.03E−01	2.10E−01	1.13
Renal cortex	4.24E−01	2.45E−01	1.19
Liver	7.19E−02	9.37E−03	4.99E−02
Lungs	5.98E−02	1.16E−02	6.57E−02
Muscle	5.47E−02	3.26E−03	1.32E−02
Ovaries	9.48E−02	7.05E−03	3.46E−02
Pancreas	8.09E−02	9.34E−03	4.64E−02
Red marrow	6.29E−02	5.04E−03	2.41E−02
Osteogenic cells	7.19E−02	1.94E−02	5.26E−02
Skin	3.97E−02	6.01E−03	3.46E−02
Spleen	7.23E−02	7.16E−03	1.64E−02
Testes	7.23E−02	6.56E−03	3.46E−02
Thymus	5.38E−02	6.29E−03	3.46E−02
Thyroid	5.07E−02	6.26E−03	3.46E−02
Urinary bladder wall	6.17E−01	2.14E−01	1.25
Uterus	1.34E−01	7.76E−03	3.46E−02
Prostate	7.64E−02	7.94E−03	4.78E−02
Salivary glands	1.78E−01	4.76E−02	2.79E−01

CONCLUSION

Biodistribution and dosimetry results suggest that ^{86}Y-**6** may provide a suitable imaging surrogate for planning and monitoring PSMA-targeted ^{90}Y- or ^{177}Lu-based radiopharmaceutical therapy.

DISCLOSURE

The costs of publication of this article were defrayed in part by the payment of page charges. Therefore, and solely to indicate this fact, this article is hereby marked "advertisement" in accordance with 18 USC section 1734. We are grateful for the following sources of support: CA148901 (SRB), CA151838 (Peter Searson, MGP), CA134675 (MGP), CA184228 (GS, MGP), and CA116477 (GS). No other potential conflict of interest relevant to this article was reported.

ACKNOWLEDGMENTS

We thank the NCI Cyclotron Research team for providing $^{86}YNO_3$. We also thank James Fox and Gilbert Green for expert technical assistance.

REFERENCES

1. Nayak TK, Brechbiel MW. ^{86}Y based PET radiopharmaceuticals: radiochemistry and biological applications. *Med Chem.* 2011;7:380–388.
2. Yoo J, Tang L, Perkins TA, et al. Preparation of high specific activity ^{86}Y using a small biomedical cyclotron. *Nucl Med Biol.* 2005;32:891–897.
3. Witzig TE, White CA, Gordon LI, et al. Safety of yttrium-90 ibritumomab tiuxetan radioimmunotherapy for relapsed low-grade, follicular, or transformed non-Hodgkin's lymphoma. *J Clin Oncol.* 2003;21:1263–1270.
4. Bodei L, Cremonesi M, Grana C, et al. Receptor radionuclide therapy with ^{90}Y-[DOTA]0-Tyr3-octreotide (^{90}Y-DOTATOC) in neuroendocrine tumours. *Eur J Nucl Med Mol Imaging.* 2004;31:1038–1046.
5. Helisch A, Forster GJ, Reber H, et al. Pre-therapeutic dosimetry and biodistribution of 86Y-DOTA-Phe1-Tyr3-octreotide versus ^{111}In-pentetreotide in patients with advanced neuroendocrine tumours. *Eur J Nucl Med Mol Imaging.* 2004;31:1386–1392.
6. Palm S, Enmon RM Jr, Matei C, et al. Pharmacokinetics and biodistribution of ^{86}Y-trastuzumab for ^{90}Y dosimetry in an ovarian carcinoma model: correlative MicroPET and MRI. *J Nucl Med.* 2003;44:1148–1155.
7. Ghosh A, Heston WD. Tumor target prostate specific membrane antigen (PSMA) and its regulation in prostate cancer. *J Cell Biochem.* 2004;91:528–539.
8. Milowsky MI, Nanus DM, Kostakoglu L, et al. Vascular targeted therapy with anti-prostate-specific membrane antigen monoclonal antibody J591 in advanced solid tumors. *J Clin Oncol.* 2007;25:540–547.
9. Olson WC, Heston WD, Rajasekaran AK. Clinical trials of cancer therapies targeting prostate-specific membrane antigen. *Rev Recent Clin Trials.* 2007;2:182–190.

10. Schülke N, Varlamova OA, Donovan GP, et al. The homodimer of prostate-specific membrane antigen is a functional target for cancer therapy. *Proc Natl Acad Sci USA.* 2003;100:12590–12595.
11. Mease RC, Foss CA, Pomper MG. PET imaging in prostate cancer: focus on prostate-specific membrane antigen. *Curr Top Med Chem.* 2013;13:951–962.
12. Banerjee SR, Pullambhatla M, Byun Y, et al. ^{68}Ga-labeled inhibitors of prostate-specific membrane antigen (PSMA) for imaging prostate cancer. *J Med Chem.* 2010;53:5333–5341.
13. Cho SY, Gage KL, Mease RC, et al. Biodistribution, tumor detection, and radiation dosimetry of ^{18}F-DCFBC, a low-molecular-weight inhibitor of prostate-specific membrane antigen, in patients with metastatic prostate cancer. *J Nucl Med.* 2012;53:1883–1891.
14. Kulkarni H, Weineisen M, Mueller D, et al. First clinical results with Lu-177 PSMA-TUM1 for the treatment of castrate-resistant metastatic prostate cancer. *J Nucl Med.* 2014;55(suppl 1):10.
15. Zechmann CM, Afshar-Oromieh A, Armor T, et al. Radiation dosimetry and first therapy results with a ^{124}I/^{131}I-labeled small molecule (MIP-1095) targeting PSMA for prostate cancer therapy. *Eur J Nucl Med Mol Imaging.* 2014;41:1280–1292.
16. Banerjee SR, Pullambhatla M, Shallal H, Lisok A, Mease RC, Pomper MG. A modular strategy to prepare multivalent inhibitors of prostate-specific membrane antigen (PSMA). *Oncotarget.* 2011;2:1244–1253.
17. Banerjee SR, Pullambhatla M, Byun Y, et al. Sequential SPECT and optical imaging of experimental models of prostate cancer with a dual modality inhibitor of the prostate-specific membrane antigen. *Angew Chem Int Ed Engl.* 2011;50:9167–9170.
18. Banerjee SR, Foss CA, Castanares M, et al. Synthesis and evaluation of technetium-99m- and rhenium-labeled inhibitors of the prostate-specific membrane antigen (PSMA). *J Med Chem.* 2008;51:4504–4517.
19. Chandran SS, Banerjee SR, Mease RC, Pomper MG, Denmeade SR. Characterization of a targeted nanoparticle functionalized with a urea-based inhibitor of prostate-specific membrane antigen (PSMA). *Cancer Biol Ther.* 2008;7:974–982.
20. Kam BL, Teunissen JJ, Krenning EP, et al. Lutetium-labelled peptides for therapy of neuroendocrine tumours. *Eur J Nucl Med Mol Imaging.* 2012;39(suppl 1): S103–S112.
21. Chen Z, Penet MF, Nimmagadda S, et al. PSMA-targeted theranostic nanoplex for prostate cancer therapy. *ACS Nano.* 2012;6:7752–7762.
22. Cheng Y, Prusoff WH. Relationship between the inhibition constant (K1) and the concentration of inhibitor which causes 50 per cent inhibition (I50) of an enzymatic reaction. *Biochem Pharmacol.* 1973;22:3099–3108.
23. Olszewski RT, Bukhari N, Zhou J, et al. NAAG peptidase inhibition reduces locomotor activity and some stereotypes in the PCP model of schizophrenia via group II mGluR. *J Neurochem.* 2004;89:876–885.
24. Schwartz J, Jaggi JS, O'Donoghue JA, et al. Renal uptake of bismuth-213 and its contribution to kidney radiation dose following administration of actinium-225-labeled antibody. *Phys Med Biol.* 2011;56:721–733.
25. Woodard HQ, Bigler RE, Freed B. Letter: expression of tissue isotope distribution. *J Nucl Med.* 1975;16:958–959.
26. Bolch WE, Eckerman KF, Sgouros G, Thomas SR. MIRD pamphlet no. 21: a generalized schema for radiopharmaceutical dosimetry—standardization of nomenclature. *J Nucl Med.* 2009;50:477–484.
27. Stabin MG, Sparks RB, Crowe E. OLINDA/EXM: the second-generation personal computer software for internal dose assessment in nuclear medicine. *J Nucl Med.* 2005;46:1023–1027.
28. Silver DA, Pellicer I, Fair WR, Heston WD, Cordon-Cardo C. Prostate-specific membrane antigen expression in normal and malignant human tissues. *Clin Cancer Res.* 1997;3:81–85.
29. Baechler S, Hobbs RF, Boubaker A, et al. Three-dimensional radiobiological dosimetry of kidneys for treatment planning in peptide receptor radionuclide therapy. *Med Phys.* 2012;39:6118–6128.
30. Hobbs RF, Wahl RL, Lodge MA, et al. ^{124}I PET-based 3D-RD dosimetry for a pediatric thyroid cancer patient: real-time treatment planning and methodologic comparison. *J Nucl Med.* 2009;50:1844–1847.
31. Ma D, McDevitt MR, Barendswaard E, et al. Radioimmunotherapy for model B cell malignancies using ^{90}Y-labeled anti-CD19 and anti-CD20 monoclonal antibodies. *Leukemia.* 2002;16:60–66.
32. Baur B, Solbach C, Andreolli E, Winter G, Machulla HJ, Reske SN. Synthesis, radiolabelling and in vitro characterization of the gallium-68-, yttrium-90- and lutetium-177-labelled PSMA ligand, CHX-A''-DTPA-DUPA-Pep. *Pharmaceuticals (Basel).* 2014;7:517–529.
33. Bander NH, Milowsky MI, Nanus DM, Kostakoglu L, Vallabhajosula S, Goldsmith SJ. Phase I trial of 177lutetium-labeled J591, a monoclonal antibody to prostate-specific membrane antigen, in patients with androgen-independent prostate cancer. *J Clin Oncol.* 2005;23:4591–4601.
34. Tagawa ST, Akhtar NH, Nikolopoulou A, et al. Bone marrow recovery and subsequent chemotherapy following radiolabeled anti-prostate-specific membrane antigen monoclonal antibody j591 in men with metastatic castration-resistant prostate cancer. *Front Oncol.* 2013;3:214.
35. Tagawa ST, Milowsky MI, Morris M, et al. Phase II study of lutetium-177-labeled anti-prostate-specific membrane antigen monoclonal antibody J591 for metastatic castration-resistant prostate cancer. *Clin Cancer Res.* 2013;19:5182–5191.
36. Vallabhajosula S, Kuji I, Hamacher KA, et al. Pharmacokinetics and biodistribution of ^{111}In- and ^{177}Lu-labeled J591 antibody specific for prostate-specific membrane antigen: prediction of ^{90}Y-J591 radiation dosimetry based on ^{111}In or ^{177}Lu? *J Nucl Med.* 2005;46:634–641.